Anal. Chem. **2007,** *79,* 2979−2983

Surface Plasmon Resonance Imaging Using a High Numerical Aperture Microscope Objective

Bo Huang,† Fang Yu, and Richard N. Zare*

Department of Chemistry, Stanford University, Stanford, California 94305-5080

We designed, constructed, and tested a surface plasmon resonance (SPR) microscope using a high numerical aperture objective from a commercially available inverted optical microscope. Such a configuration, combined with various methods to shorten the surface plasmon propagation length, achieves diffraction-limited spatial resolution in the transverse direction and near-diffraction-limited resolution in the longitudinal direction. A virtue of the objective-type SPR imaging is that we achieve distortion-free angle-resolved SPR imaging, allowing the angle-dependent reflectivity of the sample to be examined on a pixel-by-pixel basis, thus offering high-resolution information about surface properties

The surface plasmon resonance (SPR) phenomenon[1] occurs when the external light energy resonantly induces the free electrons of the metal to oscillate at a metal/dielectric interface. As a result, the radiant energy is absorbed by the metal at a certain incident angle, and the metal displays a reflectivity minimum whose angular position is extremely sensitive to the index of refraction of the dielectric medium in contact with the metal surface. Most SPR measurements are based on the Kretschmann−Raether configuration;[2] i.e., a prism is used to couple the light into the metal film. When scanning the incident angle beyond the critical angle where total internal reflection (TIR) happens, a dip of reflectivity is monitored. Using the prism configuration, it is also possible to achieve two-dimensional (2D) imaging, which is called surface plasmon resonance imaging (SPRI). Since its invention in 1988,[3] SPRI has become a powerful tool to image subtle interfacial features by means of refractive index contrast. The high sensitivity of SPRI has made it a good tool to read biomolecular binding events on, for example, DNA or protein microarrays, in a label-free fashion.[4−6]

Unfortunately, the physical constraint of the prism limits the numerical aperture (NA) and magnification of an imaging system, thus providing poor spatial resolution. For example, due to diffraction, the imaging resolution of a lens with an NA of 0.1 is ∼3 μm at a wavelength of 633 nm. The prism also distorts SPR images and causes the images to move when the incident angle is scanned. In order to correct the SPR image and improve its quality, compensating imaging optics are used, such as a double-prism geometry,[7] a cylindrical prism geometry,[8] or a tilting CCD camera. In fact, the cylindrical prism geometry introduced by Shumaker-Parry and Campbell[8] has claimed to be able to do angle-resolved SPRI of a biological microarray when the feature size is large (∼200 μm) and the lateral resolution is not critical.

We describe here an alternative approach using a high NA microscope objective to launch the SPR. This configuration is similar to the widely used through-the-objective configuration in total internal reflection fluorescence (TIRF) microscopy,[9] which solves the image distortion and movement problem. The use of a high NA and high magnification imaging system ensures that the resolution of the imaging optics is diffraction-limited (∼300 nm). In fact, this diffraction limit defines the lateral resolution of SPRI (perpendicular to the incident plane of light). However, at this high optical resolution, the longitudinal resolution (parallel to the incident plane of light) becomes limited by the propagation length of the surface plasmon, which is several micrometers in typical applications. There is a special case where Smolyaninov et al.[10] have used 2D SPR optics to magnify nanostructures on a metal surface, although its applications are limited to features on the metal film that create strong scattering of the surface plasmon. Two other groups have tried to solve the longitudinal resolution problem using a localized surface plasmon polariton excited from a wide range of azimuthal angles,[11,12] but these approaches either require a slow $x-y$ scanning process[13] or compromise image contrast owing to the existence of *s*-polarized excitation and multiple incident angles arising from the width of the mask.[12]

There exist much simpler solutions to improve the longitudinal resolution, by increasing the damping of SP waves in the metal film, thus reducing the propagation length of the surface plasmon, using a lossy metal[14] or a lossy wavelength of light.[15] We will show

* To whom correspondence should be addressed. E-mail:zare@stanford.edu.
† Current address: Department of Chemistry and Chemical Biology, Harvard University, Cambridge, MA 02138.

(1) Raether, H. *Surface Plasmons on Smooth and Rough Surfaces and on Gratings*; Springer-Verlag: Berlin, 1988.
(2) Kretschman, E.; Raether, H. *Z. Naturforsch., Part A* **1968**, *23*, 2135.
(3) Rothenhausler, B.; Knoll, W. *Nature* **1988**, *332*, 615−17.
(4) Wolf, L. K.; Fullenkamp, D. E.; Georgiadis, R. M. *J. Am. Chem. Soc.* **2005**, *127*, 17453−17459.
(5) Nelson, B. P.; Grimsrud, T. E.; Liles, M. R.; Goodman, R. M.; Corn, R. M. *Anal. Chem.* **2001**, *73*, 1−7.
(6) Shumaker-Parry, J. S.; Zareie, M. H.; Aebersold, R.; Campbell, C. T. *Anal. Chem.* **2004**, *76*, 918−929.
(7) Johansen, K. Imaging SPR Apparatus. U.S. patent 6862094, March 1, 2005.
(8) Shumaker-Parry, J. S.; Campbell, C. T. *Anal. Chem.* **2004**, *76*, 907−917.
(9) Axelrod, D. *Traffic* **2001**, *2*, 764−774.
(10) Smolyaninov, I. I.; Elliott, J.; Zayats, A. V.; Davis, C. C. *Phys. Rev. Lett.* **2005**, *94*, 1−4.
(11) Kano, H.; Mizuguchi, S.; Kawata, S. *J. Opt. Soc. Am., B* **1998**, *15*, 1381−1386.
(12) Stabler, G.; Somekh, M. G.; See, C. W. *J. Microsc. (Oxford)* **2004**, *214*, 328−333.
(13) Kano, H.; Knoll, W. *Opt. Commun.* **2000**, *182*, 11−15.

10.1021/ac062284x CCC: $37.00
Published on Web 02/20/2007

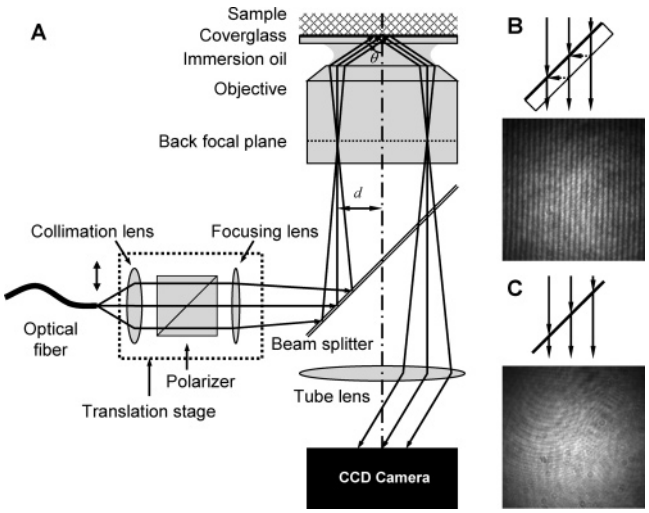

Figure 1. Principle of objective-type SPRI. (A) The optical configuration of the SPR microscope. (B) Interference patterns observed when using a dichroic mirror (565DRLPXR, Omega Filters) as the beam splitter and (C) elimination of beam splitter interferences when using a pellicle beam splitter. Both images are acquired using 638-nm laser, 1.40 NA objective, and gold-coated cover glass, with an incident angle slightly smaller than the critical of the glass/water interface.

how we adopted these solutions to improve the resolution of the objective-type SPRI. These solutions still involve the tradeoff between resolution and image contrast, which is discussed later.

EXPERIMENTAL SECTION

Setup. We constructed the SPR microscope based on an inverted microscope (Nikon TE2000-U), which is shown in Figure 1. A 638-nm diode laser (RCL-025−638, Crystalaser) and a 532-nm diode-pumped, frequency-doubled Nd:YAG laser (Compass 215M, Coherent) are combined and coupled into the same single-mode optical fiber (OZ Optics). The fiber output is collimated by an achromatic lens ($f = 100$ mm), converted to *p*-polarization with a cube polarizer, focused by an achromatic lens ($f = 400$ mm) to the back focal plane of a high numerical aperture objective (Nikon Plan Apo 100x NA 1.4, Nikon Plan Apo 60× NA 1.45, or Nikon Plan 100× NA 1.49), and finally emerged from the objective as a parallel beam. The fiber output, collimation lens, focusing lens, and necessary mirrors are mounted on a linear translation stage to adjust the offset of the laser from the optical axis of the objective. Reflected laser from the metal film enters the objective and is then imaged on to a CCD camera (I-PentaMax, Roper Scientific).

The incident angle of the laser at the metal film can be calculated through the sine condition of an aplanatic optical system:[16]

$$d = f \sin \theta \tag{1}$$

where d is the offset of the laser from the optical axis of the objective, f is the focal length of the objective, and θ is the incident angle. Although it is possible to use the absolute value of d to derive the incident angle, the calculation is usually not accurate because of imperfect alignment and aberrations in the objective. Therefore, we calibrate the incident angle with respect to the relative displacement from the critical angle or a known SPR minimum angle:

$$d - d_0 = f(\sin \theta - \sin \theta_0) \tag{2}$$

where d_0 and θ_0 are the reference offset and the reference angle, respectively.

Imaging Substrates. Microscope cover glasses (VWR) are cleaned by sonicating in 1 M KOH and then in water. Gold slides are prepared by sequentially depositing a ∼2-nm Cr layer and a ∼50-nm gold layer at a rate of 0.1 nm/s and a pressure of 1×10^{-6} Mbar using an Edwards 306 thermal evaporator. Copper slides are prepared by depositing a ∼2-nm Cr layer and a ∼30-nm copper layer at a rate of 0.1 nm/s at a pressure of 9×10^{-7} Mbar on a Veeco evaporation station. Patterned poly(dimethylsiloxane) (PDMS) stamps are fabricated using standard soft lithography techniques.

Four substrates are used for imaging:

(1) Unpatterned, metal-coated cover glass. For imaging in water, a PDMS slab with a 1 mm wide × 0.1 mm deep groove is placed on the cover glass to form a flow channel. The SPR curve is first acquired in HEPES-buffered saline (20 mM HEPES, pH 7.5, 100 mM NaCl). Then 1 mg/mL biotinylated bovine serum albumin (BSA; Pierce Biotech) is injected into the channel, incubated for 5 min, followed by buffer washing and injection of 1 mg/mL neutravidin (Pierce Biotech). The SPR curve is scanned again after a second buffer washing.

(2) Patterned PDMS stamp directly placed on a metal-coated cover glass. When the incident angle is set to the SPR minimum of air interface, the regions corresponding to the grooves in the PDMS stamp show low reflectivity, whereas the regions in contact with PDMS have high reflectivity because surface plasmons are not excited.

(3) Thiol patterns on gold surface created by microcontact printing. A 10 mM octadecanethiol in ethanol solution is applied to the PDMS stamp using a cotton swab. After the ethanol evaporates, the PDMS stamp is placed on a piece of gold-coated cover glass for 1 min, transferring the pattern on the stamp to the self-assembled thiol layer on the gold surface.

(4) Poly(tetrafluoroethylene) (PTFE) films made by spin coating a 0.9 wt % solution of Cytop PTFE (CTL-809M) dissolved in CT-SOLV 180 solvent (AGC) on gold-coated cover glass at 2000 rpm should create a PTFE film of ∼100 nm. Small pieces of PDMS obstacles are placed on the cover glass during the spin coating to make the PTFE film uneven for imaging purposes.

Angle-Resolved SPRI. For angle-resolved SPRI, a series of images are acquired with the position of the excitation laser shifting in 10-μm steps, which correspond to ∼0.3° near the critical angle of the glass/gold/air interface using a 100× objective. The SPR minimum angle of each pixel in the image stack is obtained by fitting the dip in reflectance with a quadratic function and calibrated pixel by pixel to the position of SPR minimum on a uniform gold surface. The relationship between the SPR minimum

(14) Giebel, K. F.; Bechinger, C.; Herminghaus, S.; Riedel, M.; Leiderer, P.; Weiland, U.; Bastmeyer, M. *Biophys. J.* **1999**, *76*, 509−516.
(15) Berger, C. E. H.; Kooyman, R. P. H.; Greve, J. *Rev. Sci. Instrum.* **1994**, *65*, 2829−2836.
(16) Richards, B.; Wolf, E. *Proc. R. Soc. London, Ser. A* **1959**, *253*, 358−379.

Table 1. Maximum Incident Angle, Critical Angle, and SPR Minimum Angle of Popular High NA Objective Systems

NA	$n_{substrate}$[a]	nominal θ_m (deg)	θ_c (deg)		θ_{SPR} (deg) for 638-nm excitation[b]					
					in air			in water		
			in air	in water	Au	Cu	Al	Au	Cu	Al
1.4/1.45/1.49	1.515	67.5/73.2/79.6	41.3	61.6	43.9	44.2	42.8	71.6	70.8	65.6
1.69	1.780	68.0	34.2	48.5	36.2	36.3	35.3	54.1	54.5	51.7

[a] The index of refraction of the immersion medium and the cover glass. Objectives with NA < 1.5 use conventional cover glass, and objectives with higher NA uses special cover glass with high index of refraction. [b] The complex permittivity of the metals are $-12.30 + 1.29i$ for Au, $-13.30 + 4.13i$ for Cu, $-40.34 + 15.25i$ for Al, and $-1.23 + 20.78i$ for Cr at $\lambda = 638$ nm. Thicknesses of the metal layers are 50 nm for Au (with 2-nm Cr), 30 nm for Cu (with 2-nm Cr) and 15 nm for Al.

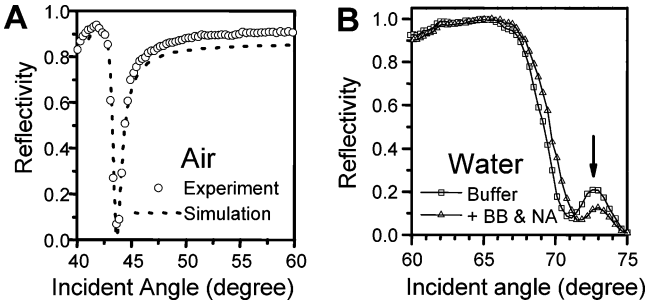

Figure 2. SPR curves measured by scanning the incident angle. Acquired using 1.45 NA objective, 638-nm excitation laser, and 50-nm gold-coated cover glass. Reflectivities are calculated by normalizing the reflected laser intensities in the CCD images so that their maximum value matches that in a theoretical SPR curve. (A) Incident angle dependence of reflectivity at glass/gold/air interface, compared with the simulation. (B) Reflectivities at glass/gold/water interface before and after binding biotin-BSA (BB) and neutravidin (NA) to the surface. The arrow indicates the incident angle when the laser beam is moving out of the objective aperture.

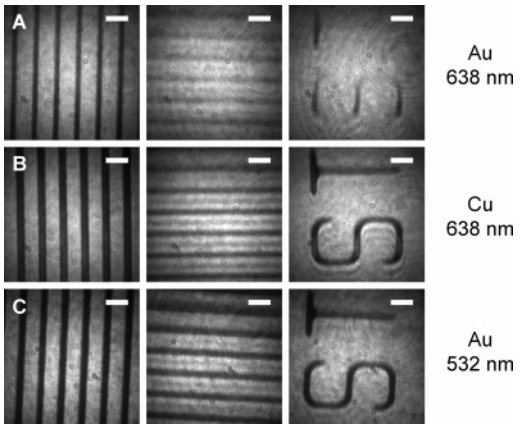

Figure 3. Resolution of SPRI. Imaging of a PDMS stamp on a (A) gold film with 638-nm laser, (B) gold film with 532-nm laser, and (C) copper film with 638-nm laser. The incident angle is set at the SPR resonance angle of glass/metal/air interface. Scale bars are 6 μm.

angle and PTFE film thickness is obtained by simulating SPR curves with different film thicknesses. All theoretical SPR curves are calculated using Fresnel's equation.[17] The parameters of the metal for the calculation are obtained from the literature.[18,19]

RESULTS AND DISCUSSION

Objective-Type SPRI. As illustrated in Figure 1A, the objective-type SPRI setup uses an immersion objective having a NA that is larger than the index of refraction of the medium. In this way, when the incident light is shifted to the edge of the objective back aperture, it will reach the sample at an angle that is larger than the critical angle. Although this SPRI setup has a configuration similar to that of objective-type TIRF microscopy, they differ in the following two aspects.

First, a TIRF microscope uses a dichroic mirror to separate the fluorescence emission from the excitation light. When imaging the coherent reflected laser in SPRI, conventional beam splitters create interference patterns in the images because of the reflections at different surfaces (Figure 1B). We solve this problem using a pellicle beam splitter (National Photocolor), which is a 2-μm-thick nitrocellulose film. As shown in Figure 1C, such a thin-film beam splitter completely eliminates the vertical stripes caused by interference. We can still observe ring-shaped interference patterns, which is common when using a coherent light source and can be removed in various ways, including the use of *s*-polarized excitation light as the reference.

Second, because SPR happens at a larger angle than the critical angle, SPRI places more demands on the NA of the objective than TIRF microscopy. The nominal maximum angles of different objectives are compared to the SPR minimum angle with different medium and metal films in Table 1. For example, an objective with a NA of 1.4 is sufficient for TIRF microscopy in water but is unable to cover the SPR minimum angle. To increase the angle coverage, metal films having a small SPR minimum angle (such as aluminum) or special objectives using substrates with high index of refraction (such as an Olympus 1.65 NA objective) can be used.

The angle dependence of the surface reflectivity can be measured by scanning the offset of the incident laser. Figure 2 shows the reflectivity curve of a 50-nm gold film measured in air and in water using 638-nm excitation. In the case of SPR in water, the incident laser is shifted from the back aperture of the 1.45 NA objective before the full dip in reflectance can be revealed. Nevertheless, this limited incident angle range does not affect SPRI because it is usually performed at an incident angle smaller than SPR minimum to address the steepest reflectivity slope and achieve good reflectivity contrast. As can be seen in Figure 2B, the shift in SPR minimum angle when adsorbing a layer of biotinylated BSA and then a layer of neutravidin can be clearly observed. Compared to the angle scanning in a conventional SPR measurement, the use of an objective lens translates the rotational motion of the incident light at the sample into a linear motion of

(17) http://www.mpip-mainz.mpg.de/~johanns/ak_knoll_Software.htm.
(18) Schulz, L. G. *J. Opt. Soc. Am.* **1954**, *44*, 362−368.
(19) Schulz, L. G. *J. Opt. Soc. Am.* **1954**, *44*, 357−362.

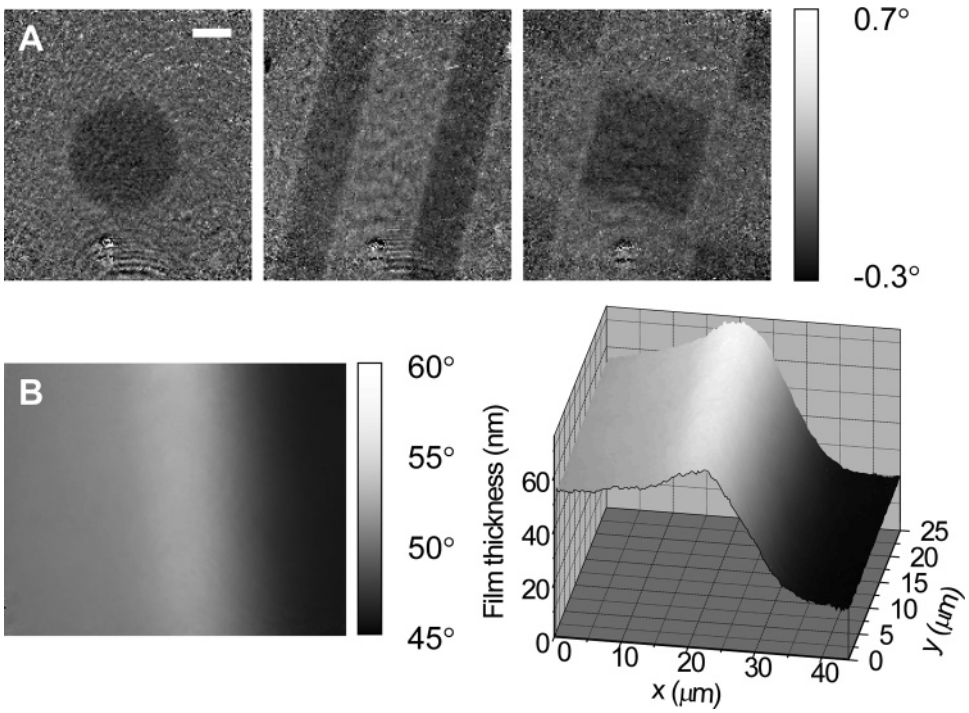

Figure 4. Angle-resolved SPR imaging (NA = 1.4): (A) images of octadecylthiol patterns stamped on a cover glass coated with a 50-nm gold film. The excitation wavelength is 532 nm. Measured SPR minimum angles are calibrated pixel by pixel against a homogeneous thiol film on the same cover glass. Images show the difference between the local SPR minimum angles and that of a glass/gold/air interface. Scale bars are 6 μm. (B) Image of an uneven PTFE film on a cover glass coated with a 50-nm gold film, acquired using 638-nm excitation. The left panel shows the SPR minimum angles in a 45 μm $\times$ 25 μm area and the right panel shows the calculated surface topography.

Table 2. Propagation Length and Refractive Index Sensitivity of SPR Excited on Gold and Copper Films at Different Wavelengths

metal	wavelength (nm)	optimal thickness (nm)	propagation length[a] (μm) in air	propagation length[a] (μm) in water	rel refractive index sensitivity[b]
gold	638	50	8.3	3.1	unity
gold	532	50	0.5	0.2	0.27
copper	638	30	3.9	1.5	0.40

[a] The calculation is based on equations in Raether's book.[1] [b] The refractive index sensitivity is the calculated slope of reflectivity increment as a function of 1-nm dielectric layer ($\epsilon = 2.1$) consecutively deposited onto the metal film in air, monitored at a fixed angle slightly smaller than the SPR minimum. The calculated sensitivities in different conditions are normalized to that of gold at 638-nm excitation.

the stage, which may simplify the system design and improve the overall mechanical performance.

When fixing the incident angle at the SPR minimum angle of air interface, images of a PDMS stamp on gold surface can be obtained. As shown is Figure 3, micrometer-sized patterns can be imaged with no noticeable distortion. Particularly, Figure 3A shows features as small as 1 μm can be revealed when the SP propagation is parallel to the edge of the patterns. On the other hand, the images are smeared in the SPR propagation direction. By switching to copper films (Figure 3B) or 532-nm excitation (Figure 3C), the image qualities are significantly improved. Table 2 shows the decrease in surface plasmon propagation length and the improvement of resolution in these conditions. It also shows that the sensitivity in index of refraction is not significantly compromised compared to the increase in resolution. In fact, theoretically, choosing a wavelength longer than 532 nm for excitation (such as 567 nm) could provide a better tradeoff between resolution and contrast.

Angle-Resolved SPRI. In most cases, SPRI monitors the reflectivity at a fixed incident angle. By scanning the incident angle, angle-resolved SPRI[4,6] obtains a full reflectivity curve, yielding more information on the surface properties. Especially, it enables the possibility to examine abnormal SPR phenomena, such as the dip broadening and minimum reflectivity drifting,[20] which may confuse the image interpretation. Such information cannot be obtained simply from SPRI studies with a fixed incident angle. In prism-type SPRI, however, the sample image moves relative to the camera when scanning the incident angle, resulting in a changing shape of the image, which complicates the data analysis and prevents the SPR curve from being obtained with higher spatial resolution.

A major advantage of objective-type SPRI is that the sample and imaging optical paths are fixed when scanning the incident angle, thus allowing even pixel-by-pixel tracking of the reflectivity in the images. In this way, a complete SPR curve can be obtained for each pixel. Figure 4A shows the images of microcontact-printed C18-thiol patterns on a gold surface, which give an SPR minimum angle difference of 0.55 $\pm$ 0.1°, obtained by fitting the SPR minimum angles from each pixel when scanning the incident angle. Assuming a refractive index of the SAM of 1.5, this angle shift corresponds to ~2 nm of thickness variation, which coincides well with the value that has been previously reported.[21] In such a

(20) Chah, S.; Kumar, C. V.; Hammond, M. R.; Zare, R. N. *Anal. Chem.* **2004**, *76*, 2112−2117.

way, each pixel generates a SPR curve and the image is constructed using the SPR minimum angle information; therefore, effects of laser intensity variations, such as the inhomogeneous profile and the interferences, are significantly reduced. By referencing using a homogeneous surface, this method also corrects the difference in incident angles at different positions of the image field due to aberrations of the objective lens.

The full SPR curve contains more information than just the reflectivity at a certain incident angle. For example, the position of the SPR minimum angle can be used to determine the thickness of a film on a surface. As a demonstration, we created an uneven PTFE film on gold-coated cover glass. Figure 4B shows that the thickness topography of the PTFE film can be determined with high spatial resolution.

CONCLUSION

An objective-type surface plasmon resonance microscope with its distortion-free, angle-resolved imaging capability is expected to extract detailed information on surface properties with nearly diffraction-limited spatial resolution. It is also simple in design because this device employs the widely used objective-type TIR configuration and only requires a small modification of modular elements. Moreover, this configuration opens the possibility for simultaneous detection of SPR signals and fluorescence signals through surface plasmon coupled emission,[22] yielding more insight into surface features and processes. Therefore, we expect that this objective-type SPRI design will find wide applications and become a useful complement to the conventional prism-type SPRI.

(21) Han, J.; Wang, X.; Kwok, D. Y. Proceedings−International Conference on MEMS, NANO and Smart Systems, ICMENS, 2004; pp 22−25.
(22) Burghardt, T. P.; Charlesworth, J. E.; Halstead, M. F.; Tarara, J. E.; Ajtai, K. *Biophys. J.* **2006**, *90*, 4662−4671.

ACKNOWLEDGMENT

This work is supported by National Science Foundation (NSF PHY-0411641).

Received for review December 1, 2006. Accepted January 22, 2007.

AC062284X